

This is the accepted manuscript made available via CHORUS. The article has been published as:

## Isotopic effects in sub-barrier fusion of Si + Si systems

G. Colucci, G. Montagnoli, A. M. Stefanini, H. Esbensen, D. Bourgin, P. Čolović, L. Corradi, M. Faggian, E. Fioretto, F. Galtarossa, A. Goasduff, J. Grebosz, F. Haas, M. Mazzocco, F. Scarlassara, C. Stefanini, E. Strano, S. Szilner, M. Urbani, and G. L. Zhang

Phys. Rev. C **97**, 044613 — Published 23 April 2018

DOI: [10.1103/PhysRevC.97.044613](https://doi.org/10.1103/PhysRevC.97.044613)

# Isotopic effects in sub-barrier fusion of Si + Si systems

G. Colucci<sup>1</sup>, G. Montagnoli<sup>1</sup>, A.M. Stefanini<sup>2</sup>, H. Esbensen<sup>3</sup>, D. Bourgin<sup>4</sup>, P. Čolović<sup>5</sup>, L. Corradi<sup>2</sup>, M. Faggian<sup>1\*</sup>, E. Fioretto<sup>2</sup>, F. Galtarossa<sup>2,6</sup>, A. Goasduff<sup>1</sup>, J. Grebosz<sup>7</sup>, F. Haas<sup>4</sup>, M. Mazzocco<sup>1</sup>, F. Scarlassara<sup>1</sup>, C. Stefanini<sup>1</sup>, E. Strano<sup>1</sup>, S. Szilner<sup>5</sup>, M. Urbani<sup>1†</sup>, G.L. Zhang<sup>1,8</sup>

<sup>1</sup> *Dipartimento di Fisica e Astronomia, Università di Padova,  
and INFN, Sez. di Padova, I-35131 Padova, Italy*

<sup>2</sup> *INFN, Laboratori Nazionali di Legnaro, I-35020 Legnaro (Padova), Italy*

<sup>3</sup> *Physics Division, Argonne National Laboratory, Argonne, IL 60439, USA*

<sup>4</sup> *IPHC, CNRS-IN2P3, Université de Strasbourg, F-67037 Strasbourg Cedex 2, France*

<sup>5</sup> *Ruđer Bošković Institute, HR-10002 Zagreb, Croatia*

<sup>6</sup> *Dipartimento di Fisica e Scienze della Terra, Univ. di Ferrara, Ferrara, Italy*

<sup>7</sup> *Institute of Nuclear Physics, Polish Academy of Sciences, PL 31-342 Cracow, Poland*

<sup>8</sup> *School of Physics and Nucl. Energy Engineering, Beihang University, Beijing 100191, China*

(Dated: April 10, 2018)

**Background:** Recent measurements of fusion cross sections for the  $^{28}\text{Si} + ^{28}\text{Si}$  system revealed a rather unsystematic behavior, i.e. they drop faster near the barrier than at lower energies. This was tentatively attributed to the large oblate deformation of  $^{28}\text{Si}$  because Coupled-Channels (CC) calculations largely underestimate the  $^{28}\text{Si} + ^{28}\text{Si}$  cross sections at low energies, unless a weak imaginary potential is applied, probably simulating the deformation.  $^{30}\text{Si}$  has no permanent deformation and its low-energy excitations are of vibrational nature. Previous measurements of this system reached only 4 mb, which is not sufficient to obtain information on effects that should show up at lower energies.

**Purpose:** The aim of the present experiment was twofold: 1) to clarify the underlying fusion dynamics by measuring the symmetric case  $^{30}\text{Si} + ^{30}\text{Si}$  in an energy range from around the Coulomb barrier to deep sub-barrier energies, and 2) to compare the results with the behaviour of  $^{28}\text{Si} + ^{28}\text{Si}$  involving two deformed nuclei.

**Methods:**  $^{30}\text{Si}$  beams from the XTU Tandem accelerator of INFN-Laboratori Nazionali di Legnaro were used, bombarding thin metallic  $^{30}\text{Si}$  targets ( $50\mu\text{g}/\text{cm}^2$ ) enriched to 99.64% in mass 30. An electrostatic beam deflector allowed the detection of fusion evaporation residues (ER) at very forward angles, and angular distributions of ER were measured.

**Results:** The excitation function of  $^{30}\text{Si} + ^{30}\text{Si}$  has been measured down to the level of a few  $\mu\text{b}$ . It has a regular shape, at variance with the unusual trend of  $^{28}\text{Si} + ^{28}\text{Si}$ . The extracted logarithmic derivative does not reach the  $L_{CS}$  limit at low energies, so that no maximum of the S-factor shows up. CC calculations were performed including the low-lying  $2^+$  and  $3^-$  excitations.

**Conclusions:** Using a Woods-Saxon (WS) potential the experimental cross sections at low energies are over-predicted, and this is a clear sign of hindrance, while the calculations performed with a M3Y + repulsion potential nicely fit the data at low energies, without the need of an imaginary potential. The comparison with the results for  $^{28}\text{Si} + ^{28}\text{Si}$  strengthens the explanation of the oblate shape of  $^{28}\text{Si}$  being the reason of the irregular behavior of that system.

PACS Numbers: 25.70.Jj, 24.10.Eq

## I. INTRODUCTION

The comparison of fusion data for neighbouring systems is a sensitive tool to evidence the influence of nuclear structure on reaction dynamics at energies near and below the Coulomb barrier. A comparative study was recently performed for the Si+Si systems [1], where the interest originated from the different shape of the silicon isotopes. Indeed,  $^{28}\text{Si}$  is strongly deformed with an oblate shape while  $^{30}\text{Si}$  is nearly spherical. In that work the fusion of the asymmetric system  $^{28}\text{Si} + ^{30}\text{Si}$  [1, 2] was

explained by considering one- and successive two-neutron transfer channels in the coupling scheme. The case of  $^{28}\text{Si} + ^{28}\text{Si}$  involving deformed nuclei shows an unusual behaviour, where the cross section is hindered [3] just below the barrier and then enhanced at lower energies, as shown in the comparison with the CC calculations. It was further surprising that the low-energy data were well reproduced only by artificially applying a weak, short-ranged imaginary potential, probably simulating the effect of the oblate deformation.

The nucleus  $^{30}\text{Si}$  has a spherical shape, because the measured quadrupole moment of the  $2^+$  state,  $Q_2 = -0.05(6)$  barn, is consistent with zero [4]. An attractive comparison could therefore be done between  $^{30}\text{Si} + ^{30}\text{Si}$  and  $^{28}\text{Si} + ^{28}\text{Si}$  because no transfer channels with positive Q-values exist for both cases. However, the excitation function of  $^{30}\text{Si} + ^{30}\text{Si}$  was measured only down to  $\simeq 4$  mb [5], and this prevents a meaningful comparison between the two systems. A further point of interest is the possible appearance of the hindrance phenomenon in

---

\*Present address: SUPA, Physics Department and Institute for Complex Systems and Mathematical Biology, King's College, University of Aberdeen, AB24 3UE, UK

†Present address: Department of Electrical Engineering, Universitat Politècnica de Catalunya, BarcelonaTech (UPC) Terrassa (Barcelona), Spain

this system which has a positive Q-value for fusion (+15.6 MeV) that is similar to the case of  $^{28}\text{Si}+^{30}\text{Si}$  (14.3 MeV) where an S factor maximum has almost been reached at the lowest experimental energy, see Fig. 3 of Ref. [2]. Therefore, a fusion experiment has been recently carried out at Laboratori Nazionali di Legnaro (LNL) with the purpose to extend the data of  $^{30}\text{Si}+^{30}\text{Si}$  down to energies deeply below the Coulomb barrier.

Preliminary data have already been presented at International Conferences [6, 7]. In this work we present the results of the full measurement, from well below to well above the Coulomb barrier. Section II describes the experimental set-up and the analysis procedure, while the results of CC calculations are presented in Section III. A comparison with the near-by system  $^{28}\text{Si}+^{28}\text{Si}$  follows in Section III B. The work is summarised and concluded in Section IV.

## II. EXPERIMENTAL SET-UP AND RESULTS

Beams of  $^{30}\text{Si}$  in the energy range of 47-90 MeV, with intensities of 15-30 pA, were provided by the XTU Tandem accelerator of the Laboratori Nazionali di Legnaro (LNL) of Istituto Nazionale di Fisica Nucleare INFN. The targets consisted of  $50\text{ }\mu\text{g}/\text{cm}^2$   $^{30}\text{Si}$  evaporated on  $30\text{ }\mu\text{g}/\text{cm}^2$  carbon backings facing the beam. The isotopic enrichment of  $^{30}\text{Si}$  was 99.64%. The fusion yields were not essentially affected by the small residual contaminations of  $^{29}\text{Si}$  and  $^{28}\text{Si}$  because of their higher Coulomb barriers with respect to  $^{30}\text{Si}$ . The carbon backing and the silicon target itself introduced an average beam energy loss of around 750-850 keV, which was taken into account in the analysis.

Fusion cross sections have been determined by direct detection of the fusion evaporation residues (ER) at small angles by separating out the beam and beam-like particles using the electrostatic beam deflector of LNL, that allows fast and reliable measurements of relative and absolute cross sections [1, 8]. The ER were identified downstream of the deflector by a double Time-of-Flight (ToF)  $\Delta E$ -Energy telescope composed of two micro-channel plate time detectors (MCP) followed by a transverse field ionisation chamber (IC) and by a silicon detector placed in the same gas ( $\text{CH}_4$ ) volume of the IC. The silicon detector measured the residual energy of the ER and gave the start signal for the two ToF as well as the trigger for the data acquisition. We report in Fig. 1 representative examples of two-dimensional plots  $\Delta E$ -ToF where ER can be easily recognised both near and much below the Coulomb barrier. These spectra were collected in twenty minutes and in eight hours of beam time, respectively, with comparable beam intensities.

A good separation of ER events from the residual beam-like particles is achieved at energies both above and below the Coulomb barrier. Four silicon detectors were placed symmetrically around the beam direction at the same scattering angle  $\theta_{lab} = 16^\circ$ , used to monitor

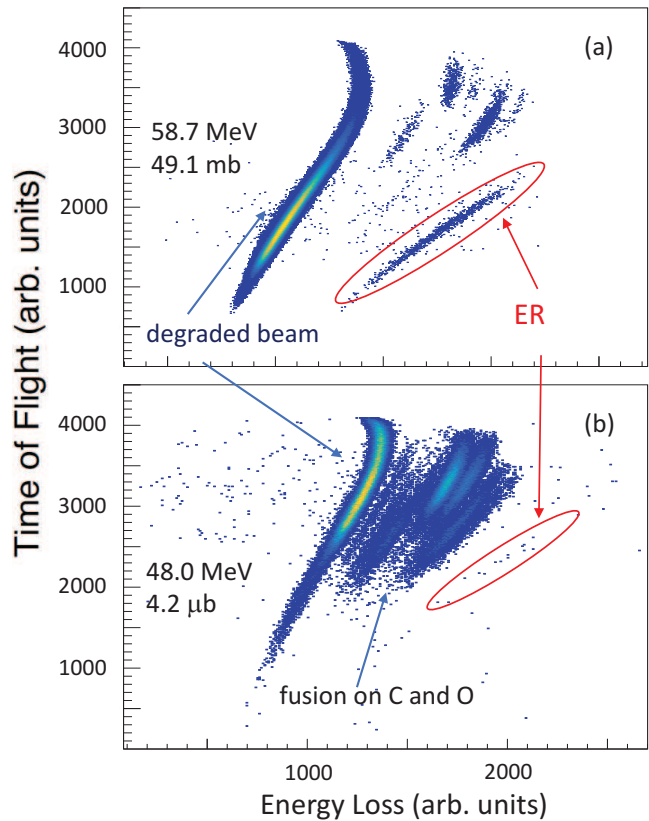


FIG. 1: (Color online) Two-dimensional spectra of Time of Flight vs. Energy loss measured at different beam energies around (a) and far below the Coulomb barrier (b), for  $^{30}\text{Si}+^{30}\text{Si}$ . The nominal beam energies and the corresponding fusion cross sections are reported. The detected events within the oval shapes are identified as fusion evaporation residues (ER) and are indicated by the red arrows. They are well separated from the other kind of events due to degraded beam and to fusion on carbon and oxygen present in the target.

the beam and to normalise the fusion yields to the Mott scattering cross section. Three ER angular distributions were measured at the energies of 58, 72 and 80 MeV in the range from  $-6^\circ$  to  $+9^\circ$ . We observed that their shape does not appreciably change with energy, in agreement with several other cases that have been studied in the past (see e.g. Refs. [9, 10]). This enables the ratio of the differential cross section to the total fusion cross section to be accurately estimated at any energy, so that we have obtained total fusion cross sections by integrating those distributions, and by simple interpolations or extrapolations for all other energies where ER measurements were taken only at  $2^\circ$  (or  $3^\circ$  for low energies). The error on the cross sections for the energies where no angular distribution was measured is not essentially increased by this procedure. We point out that the statistical uncertainty is anyway dominant from the barrier down, which is the range of energies relevant for the physical issues

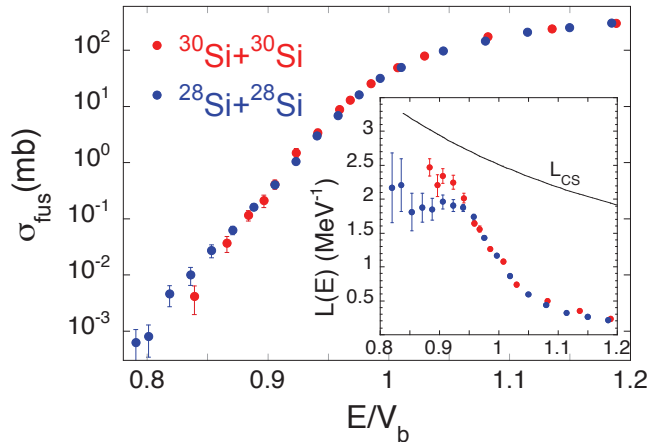


FIG. 2: (Color online) Fusion excitation function of  $^{30}\text{Si}+^{30}\text{Si}$  measured in this work, compared to the system  $^{28}\text{Si}+^{28}\text{Si}$  [1]. The energy scale is normalized to the Akyüz-Winther Coulomb barrier [11]. The reported errors are purely statistical uncertainties. The insert shows the logarithmic derivatives (slopes) of the excitation functions for the two systems.

investigated in this work.

The absolute cross section scale may be fixed, as in previous experiments using the same set-up, by the knowledge of the relevant detector solid angles, of the deflector transmission, and by the angular distribution integrations. Overall, the uncertainties affecting these quantities normally introduce a  $\pm 7\text{-}8\%$  error in that absolute scale. In the present case, however, the silicon detector at the end of the telescope had to be replaced during the measurements with a new one having a different active area, due to an unexpected failure of the old one. This introduced a not negligible additional uncertainty (probably  $\simeq 10\%$ ) in the derivation of the absolute fusion cross sections. Therefore, we have found it more reliable to normalize the present data to the previous results of Bozek et al. [5] above the barrier. All cross sections, logarithmic derivatives, S factors reported in the following of this paper derive from the normalization of the scale we decided to perform at  $E_{c.m.} = 34.9$  MeV, since this energy is common to the present and the previous experiments. At this energy the cross section quoted in Ref. [5] is  $469 \pm 60$  mb, so that the absolute cross section scale in the present work is affected by the same uncertainty ( $\pm 13\%$ ). However, only statistical errors influence the relative cross sections.

The full set of fusion cross sections measured for  $^{30}\text{Si}+^{30}\text{Si}$  in this work are reported in Fig. 2, where we noticed that the excitation function has been extended down to  $\simeq 4 \mu\text{b}$ . In the same figure a comparison is done with the existing excitation function of  $^{28}\text{Si}+^{28}\text{Si}$  [1] in a reduced energy scale. The two excitation functions appear to have different trends below the barrier. Indeed, as anticipated in the Introduction, the cross sec-

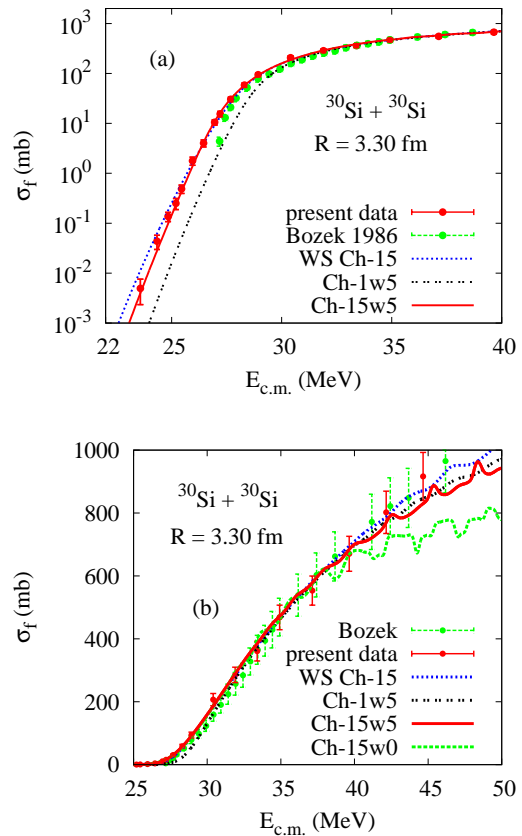


FIG. 3: Logarithmic (a) and linear plot (b) of the present and previously measured (Bozek et al., Ref. [5]) fusion cross sections for  $^{30}\text{Si}+^{30}\text{Si}$ . The data are compared to Ch-1 and Ch-15 CC calculations that are based on the M3Y+repulsion potential with parameters  $a_r = 0.38$  fm and the radius  $R = 3.30$  fm of the neutron density. Also shown are the results of Ch-15 calculations that use a WS potential with parameters  $R = 7.177$  fm,  $U_0 = -55.37$  MeV, and  $a = 0.637$  fm. The radius  $R$  was adjusted to reproduce the data at energies above the Coulomb barrier. The calculation Ch-15w0 shown in (b) illustrates the importance of an imaginary potential at high energies.

tions of the lighter system drop faster just below the barrier than at lower energies. On the contrary, the excitation function measured for  $^{30}\text{Si}+^{30}\text{Si}$  in the present work has a smoother behaviour in the whole sub-barrier energy range.

The insert of Fig. 2 shows the logarithmic derivatives (slopes) of the excitation functions for the two systems. In either case, the slopes do not cross the  $L_{CS}$  value expected for a constant astrophysical S factor. This would phenomenologically suggest the absence of hindrance [3] in the measured energy range, and this was claimed in the analysis of Ref. [7]. However a comparison with full CC calculations is necessary to confirm or disprove that evidence. This was already performed for  $^{28}\text{Si}+^{28}\text{Si}$  in Refs. [1, 13] and the following section shows the results

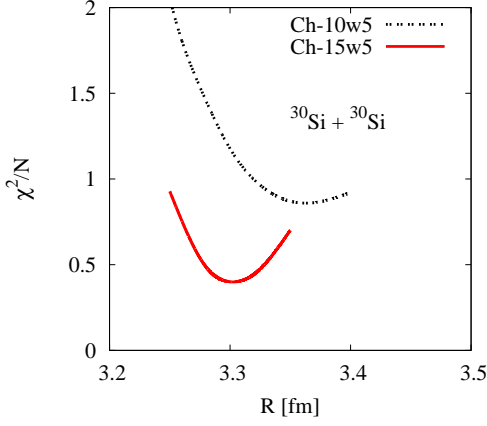


FIG. 4:  $\chi^2$  analysis of the present data by Ch-10w5 and Ch-15w5 calculations, respectively, as functions of the radius  $R$  of the neutron density in  $^{30}\text{Si}$ . The data have been normalised to Bozek's data [5] at 34.9 MeV.

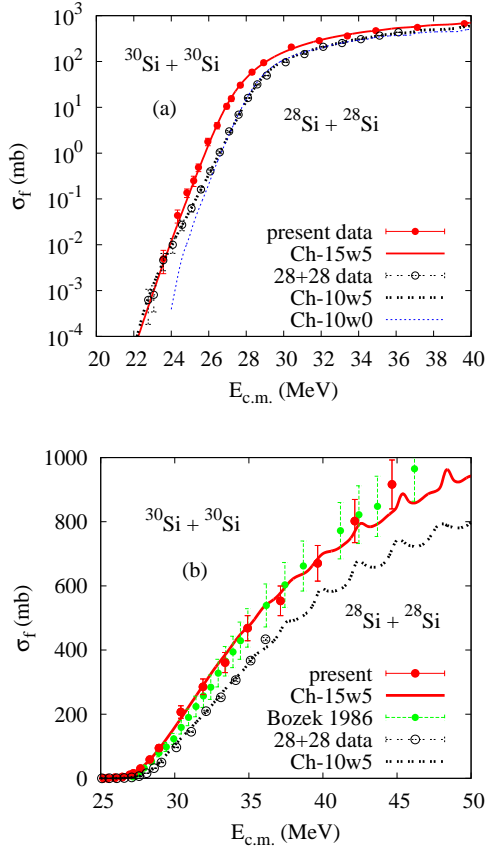


FIG. 5: Logarithmic (a) and linear plot (b) of the best fits to the  $^{28}\text{Si}+^{28}\text{Si}$  [1] and the present  $^{30}\text{Si}+^{30}\text{Si}$  fusion data obtained in Ch-10w5 and Ch-15w5 calculations, respectively.

TABLE I: Results of the analysis of the present  $^{30}\text{Si}+^{30}\text{Si}$  fusion data. The Ch-10w5 and Ch-15w5 calculations include 10 and 15 channels, respectively, and an imaginary potential with depth  $w=-5$  MeV, radius  $R_w = 6.63$  fm, and diffuseness  $a_w = 0.2$  fm. A systematic error of 5 % was adopted in the analysis. The radius  $R$  of the neutron density was adjusted in each case to minimize the  $\chi^2$ , whereas the charge radius was kept fixed at 3.165 fm (see Table II). The minimum of the pocket,  $V_{min}$ , and the height of the Coulomb barrier,  $V_{CB}$ , are also shown. Similar results are shown for  $^{28}\text{Si}+^{28}\text{Si}$  [1, 13].

Reaction	$a_w$ (fm)	$R$ (fm)	$V_{min}$	$V_{CB}$	$\chi^2/N$
$^{30}\text{Si}+^{30}\text{Si}$ Ch-10w5	0.2	3.35	19.52	28.42	0.87
$^{30}\text{Si}+^{30}\text{Si}$ Ch-15w5	0.2	3.30	18.85	28.51	0.40
$^{28}\text{Si}+^{28}\text{Si}$ Ch-10w5[1]	0.2	3.135	23.76	29.37	1.71
$^{28}\text{Si}+^{28}\text{Si}$ Ch-10w5[13]	0.3	3.125	23.59	29.41	1.16

TABLE II: Radius  $R$  and diffuseness  $a$  of the proton and neutron densities in  $^{28}\text{Si}$  and  $^{30}\text{Si}$ . The proton densities (the first and the fourth line) were adjusted to reproduce the known point-proton rms-radii [14]. The proton+neutron densities were used to calculate the M3Y + repulsion potential [12]. The radii of the neutron density of  $^{30}\text{Si}$  shown in line 2 and 3 were obtained by optimizing the fit to the present  $^{30}\text{Si}+^{30}\text{Si}$  fusion data in Ch-10w5 and Ch-15w5 calculations, respectively. Similar results were obtained for  $^{28}\text{Si}$  in Refs. [1, 13] from the analysis of the  $^{28}\text{Si}+^{28}\text{Si}$  fusion data. The parameter  $a_w$  is the adopted diffuseness of the imaginary potential.

Source	$a_w$ (fm)	$R$ (fm)	$a$ (fm)	rms	rms(pp)	rms(ch)
$^{30}\text{Si}$ [14]		3.165	0.48	3.032	3.032(4)	3.133(4)
Ch-10w5	0.2	3.35	0.48	3.149	fusion	new data
Ch-15w5	0.2	3.30	0.48	3.117	fusion	new data
$^{28}\text{Si}$ [14]		3.141	0.48	3.018	3.018(2)	3.122(2)
Ch-10w5	0.2	3.135	0.48	3.013	fusion	Ref.[1]
Ch-10w5	0.3	3.125	0.48	3.007	fusion	Ref.[13]

of analogous calculations for  $^{30}\text{Si}+^{30}\text{Si}$ .

### III. RESULTS OF COUPLED-CHANNELS CALCULATIONS

#### A. The system $^{30}\text{Si}+^{30}\text{Si}$

We have performed CC calculations for  $^{30}\text{Si}+^{30}\text{Si}$  using the M3Y+repulsion potential that was introduced in Ref. [12]. The nuclear structure information on the low-lying  $2^+$  and  $3^-$  states was listed in Table I of Ref. [1]. If we include all of the one- and two-phonon excitations as well as mutual excitations that can be generated by those states, we obtain a total of 15 channels (including the elastic channel). Such calculations are referred to as Ch-15 calculations and are discussed later on.

The two-phonon excitations of the  $3^-$  states have an energy that is larger than 9-10 MeV. If we exclude them,

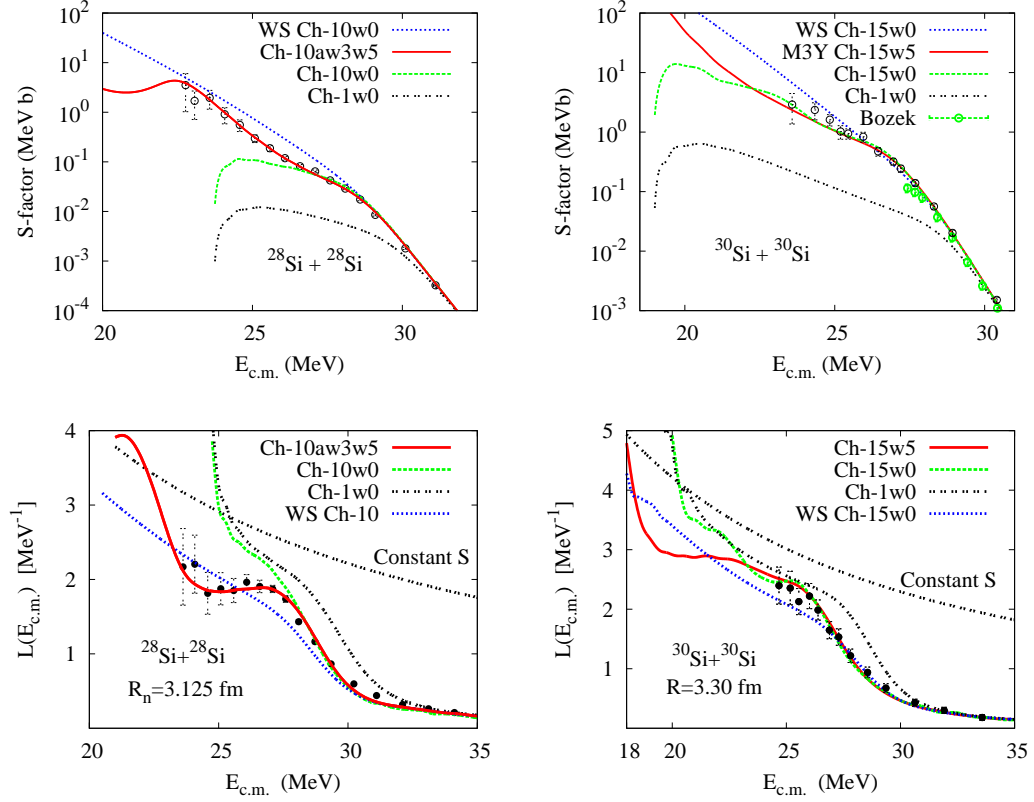


FIG. 6: S factors (upper panels) and logarithmic slopes of the excitation functions (lower panels) for the fusion of  $^{28}\text{Si} + ^{28}\text{Si}$  [1] and  $^{30}\text{Si} + ^{30}\text{Si}$  (see also Ref. [5]) are compared to the best Ch-10 and Ch-15 calculations, respectively, with (w5) and without (w0) an imaginary potential. Ch-1w0 calculations (no coupling results) are reported for reference. Results that are based on a WS potential (adjusted to reproduce the high-energy data) are also shown.

the number of channels is reduced to 12. If we also exclude the mutual excitation of the  $2^+$  and  $3^-$  states in the same nucleus, the total number of channels is reduced to 10. We have performed such Ch-10 calculations in a previous work [1] where we compared them to the existing data for  $^{28}\text{Si} + ^{28}\text{Si}$  [1] and  $^{30}\text{Si} + ^{30}\text{Si}$  [5]. We have repeated them here in an analysis of the present new data for  $^{30}\text{Si} + ^{30}\text{Si}$ .

Since  $^{30}\text{Si}$  is spherical, the CC calculations for  $^{30}\text{Si} + ^{30}\text{Si}$  are more robust than for  $^{28}\text{Si} + ^{28}\text{Si}$  because the location of the minimum of the potential pocket is essentially the same in all reaction channels. One can therefore impose the ingoing-wave boundary conditions for fusion at one common pocket minimum. This is not so easy for  $^{28}\text{Si} + ^{28}\text{Si}$  because the pocket minima are located at different radial separations. The problem was solved in Refs. [1, 13] by applying an imaginary potential with a diffuseness of  $a_w = 0.2$  to  $0.3$  fm.

However, it turns out (as is often the case see e.g. Fig. 11 of Ref. [15]) that we need a short-ranged imaginary potential in order to explain the data at high energies. The Ch-10w5 and Ch-15w5 calculations include such a weak imaginary potential, parametrised as a simple Woods-Saxon well with depth  $w_0 = -5$  MeV, radius

$R_w = 6.63$  fm, and diffuseness  $a_w = 0.2$  fm. The results of the best Ch-15w5 calculations are compared with the data in Fig. 3. It is seen in Fig. 3(b) that the calculations reproduce the high energy data much better than the Ch-15w0 calculations that do not include any imaginary potential. No coupling calculations (Ch-1w5) are also reported in Fig. 3.

The present  $^{30}\text{Si} + ^{30}\text{Si}$  data are analysed in terms of the  $\chi^2$  per data point ( $\chi^2/N$ ). The best fit to the data in each set of calculations is obtained by adjusting the radius of the neutron density that is used to calculate the M3Y+repulsion double-folding potential. The proton density, on the other hand, is kept fixed with the radius  $R = 3.165$  fm and the diffuseness  $a = 0.48$  fm. These values are consistent with the experimental point-proton RMS radius of  $^{30}\text{Si}$  (see the first line of Table II.) In general, the point-proton density is very well established by the measured RMS charge radius, whereas the point-neutron density is more uncertain. It is therefore natural to adopt the known point-proton density, whereas the point-neutron density can be determined by optimizing the fit to the fusion data.

The diffuseness of the density associated with the repulsive part of the M3Y+repulsion interaction was set to

$a_r = 0.38$  fm. The Ch-15w5 calculations are smoother and rise more steeply at high energies than the Ch-15w0 calculations where no imaginary potential is applied. This can be seen in Fig. 3(b)). The calculations that include absorption do exhibit some structures at high energies. These structures can be associated with the individual centrifugal barriers that we discussed in previous works [13, 15].

The results of the analysis that is based on Ch-10w5 and Ch-15w5 calculations, respectively, are shown in line 1 and 2 of Table I. The results were obtained by minimising the  $\chi^2/N$  for each set of calculations with respect to the radius  $R$  of the neutron density. The radial dependence of the  $\chi^2/N$  that were used to determine the best fits in Ch-10w5 and Ch-15w5 calculations are illustrated in Fig. 4.

It is interesting to note that the adjusted value of the neutron density radius obtained in Ch-15w5 is smaller than in Ch-10w5 calculations. The difference is of the order of 0.05 fm. The reason for this is that the smaller radius obtained in Ch-15 calculations is compensated by the polarisation of high-lying states that are included in Ch-15 calculations but not in Ch-10 calculations.

Another observation in Table I is that the  $\chi^2/N$  is much improved in the Ch-15w5 calculations compared to the result of the Ch-10w5 analysis. The reason is that the enhancement of sub-barrier fusion is larger in Ch-15 calculations than in Ch-10, and such an enhancement is evidently preferred by the data. We will therefore only show the results of Ch-15w5 calculations in the following. By the comparison of the best fit with the data in Fig. 3, it is seen that the Ch-15w5 results are in excellent agreement with the data.

The analogous Ch-15 results using a standard Woods-Saxon (WS) potential are also shown in Fig. 3. The radius of the potential,  $R = 7.177$  fm, was adjusted so that the data were reproduced at energies above the Coulomb barrier. It is seen that the data are suppressed compared to this calculation at the lowest energies which is a sign of the fusion hindrance phenomenon [3]. The suppression is evidently removed by applying the adjusted M3Y+repulsion potential as illustrated in Fig. 3(a).

### B. Comparison of results for the two systems

The analysis of the  $^{28}\text{Si}+^{28}\text{Si}$  fusion data [1] that was performed in Refs. [1, 13] was based on Ch-10 calculations. The results are listed in line 3 and 4 of Table I. It was found that the fit to the data could be improved by increasing the diffuseness  $a_w$  of the imaginary potential, from 0.2 to 0.3 fm. The need for a larger diffuseness was justified by the large deformation of  $^{28}\text{Si}$  (see Ref. [1] for details). We will therefore in the following show the results of these calculations that are denoted Ch-10aw3w5.

The excitation functions for  $^{28}\text{Si}+^{28}\text{Si}$  and  $^{30}\text{Si}+^{30}\text{Si}$  are compared in Fig. 5. The best fit to the  $^{28}\text{Si}+^{28}\text{Si}$  data was obtained in Ch-10aw3w5 calculations and is

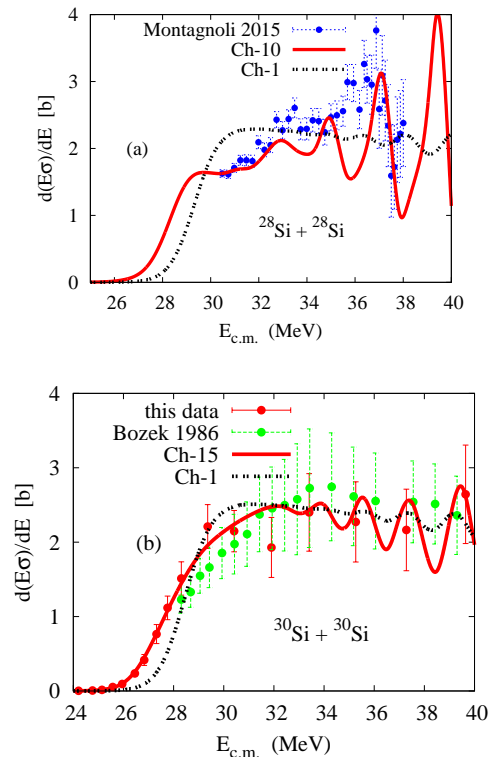


FIG. 7: The first derivative of the energy-weighted cross section for the fusion of  $^{28}\text{Si}+^{28}\text{Si}$  (Montagnoli et al., Ref. [13]) (a) and  $^{30}\text{Si}+^{30}\text{Si}$  (b) (present data and Ref. [5]) are compared to the best Ch-10aw3w5 and Ch-15w5 calculations, respectively. The results of Ch-1 calculations are also shown.

seen to be in excellent agreement with the data at all energies. The calculation Ch-10w0 that does not include any imaginary potential is also shown in Fig. 5(a), and it is seen to underpredict the data substantially at low energies.

We showed in Ref. [13] that the structures in the high energy fusion of  $^{28}\text{Si}+^{28}\text{Si}$  are strongly influenced by coupled-channels effects. On the other hand, the structures are much weaker in the no-coupling calculations. Since the couplings (both quadrupole and octupole) are much weaker in the  $^{30}\text{Si}+^{30}\text{Si}$  reaction (see Table I of Ref. [1]), it is therefore not surprising that the structures shown in Fig. 5 (b) are different and even weaker in the fusion of  $^{30}\text{Si}+^{30}\text{Si}$ .

A detailed comparison of the S factors for fusion and the logarithmic derivatives of both systems is shown in Fig. 6. We point out that the logarithmic derivative is insensitive to the absolute normalization of the cross section. The good agreement between the best calculation and the data shows that the shape of the calculated excitation function is consistent with the shape of the measured cross sections.

Another interesting feature observed in Fig. 6 is that the calculations Ch-15w0 and Ch-15w5 are both in good agreement with the data for  $^{30}\text{Si}+^{30}\text{Si}$  at low energies (see

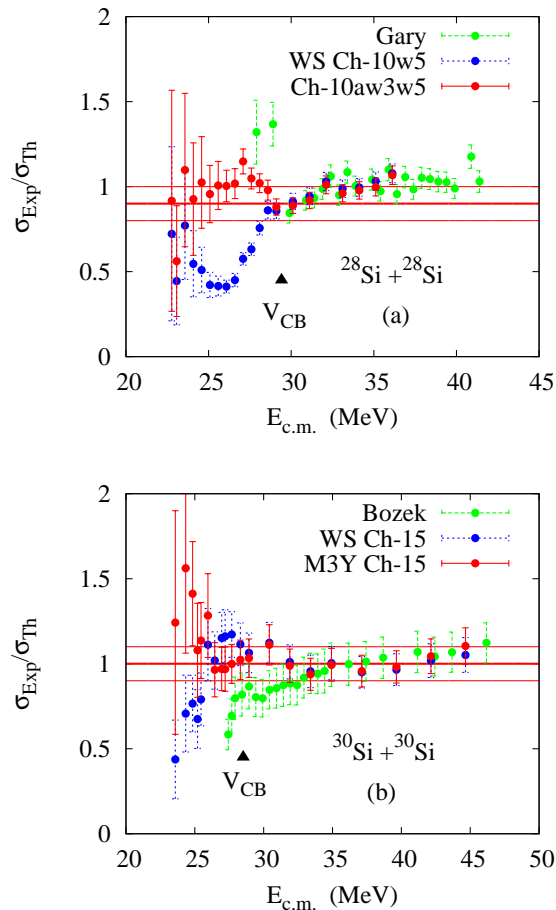


FIG. 8: Ratio of the measured and the calculated cross sections shown in Fig. 5(b) for  $^{28}\text{Si}+^{28}\text{Si}$  (a) and  $^{30}\text{Si}+^{30}\text{Si}$  (b). The ratio to the WS calculations indicates a fusion hindrance just below the Coulomb barrier for  $^{28}\text{Si}+^{28}\text{Si}$ , but that effect is seen to disappear at lower energies (the older data of Gary are from Ref. [16]). For  $^{30}\text{Si}+^{30}\text{Si}$  a fusion hindrance appears at the lowest measured energies.

the right panels), whereas the Ch-10-w0 and Ch-10w5 for  $^{28}\text{Si}+^{28}\text{Si}$  (left panels) differ substantially from each other at the lowest energies and only the Ch-10aw3w5 calculation is able to reproduce the data. These features are consistent with the spherical nature of  $^{30}\text{Si}$  and the deformation of  $^{28}\text{Si}$ .

Indeed, the deformation of  $^{28}\text{Si}$  produces barriers at different radial separations in the excited channels, as discussed in Ref. [1]. Those calculations were performed by imposing the ingoing-wave boundary conditions at the barrier of the elastic channel but the imaginary potential made it possible to probe the barriers that were located at different separations. The barriers in Fig. 4(b) of Ref. [1] associated with the excitations of the spherical nucleus  $^{30}\text{Si}$ , on the other hand, are located essentially at the same radial separation, and a weak imaginary potential was therefore not expected to have an effect. It does have some influence as illustrated in Fig. 6 of this paper but

the difference sets in at much lower energies.

The first derivatives of the energy-weighted cross sections are shown in Fig. 7. The structures observed in the fusion of  $^{28}\text{Si}+^{28}\text{Si}$  are associated with the centrifugal barriers in the entrance channel potential, although CC effects do smear out the correlation between a particular barrier and a peak in the first derivative of the energy-weighted cross sections as discussed in Ref. [13]. It is seen that the calculated structures for  $^{30}\text{Si}+^{30}\text{Si}$  are weaker so the possibility of observing these structures experimentally is not so promising.

Fig. 8 reports the ratio of the measured and the calculated cross sections that are shown in Fig. 5. Also shown are the ratios of the data to the calculations that are based on a WS potential. It is seen that the  $^{28}\text{Si}+^{28}\text{Si}$  data are suppressed or hindered at energies that are slightly below the Coulomb barrier compared to the Ch-10 calculation that uses a WS potential. However, the hindrance disappears at the lowest energies. This unusual behavior is ascribed to the large deformation of  $^{28}\text{Si}$ . The data can evidently be reproduced as discussed in Ref. [13] by using the M3Y+repulsion potential and an imaginary potential with the diffuseness  $a_w = 0.3$  fm.

On the contrary, it appears from Fig. 8 that the data for  $^{30}\text{Si}+^{30}\text{Si}$  agree with the WS calculation slightly below the barrier and become suppressed only at the lowest energies. This is the “normal” evidence of the fusion hindrance phenomenon that was first introduced in Ref. [3].

#### IV. SUMMARY

The excitation function of  $^{30}\text{Si}+^{30}\text{Si}$  has been measured down to the level of a few  $\mu\text{b}$  using the  $^{30}\text{Si}$  beams from the XTU Tandem accelerator of INFN-LNL, and an experimental set-up with an electrostatic beam deflector, allowing to detect the ER at small angles. The excitation function displays a regular behaviour, at variance with the unusual trend of the near-by case  $^{28}\text{Si}+^{28}\text{Si}$ . The extracted logarithmic derivative does not reach the  $L_{CS}$  limit at low energies, so the experimental S factor does not reach a maximum.

Coupled-Channels calculations were performed taking into account the one- and two-phonon as well as mutual excitations of the low-lying  $2^+$  and  $3^-$  states in projectile and target. Using a Woods-Saxon potential the experimental cross sections are over-predicted at low energies, so that we have evidence of the hindrance effect. The analogous calculations performed with a M3Y+repulsion potential reproduce the excitation function very well, in its whole measured energy range. A weak imaginary potential is necessary to fit the high energy cross sections, but not below the barrier as it was needed for  $^{28}\text{Si}+^{28}\text{Si}$  where the hindrance, observed just below the barrier, disappears at the lowest energies. This was ascribed to the large oblate deformation of  $^{28}\text{Si}$ , and this interpretation is reinforced by the different behavior of the symmetric system involving  $^{30}\text{Si}$  that is a spherical nucleus.

## V. ACKNOWLEDGMENTS

We are very grateful to the XTU Tandem staff, and to M.Loriggiola for preparing targets of excellent quality. The research leading to these results has received funding from the the European Union Seventh Framework

Programme FP7/2007- 2013 under Grant Agreement No. 262010 - ENSAR. This work has been supported in part by Croatian Science Foundation under the project 7194. H.E. is supported by the US Department of Energy, Office of Science, Office of Nuclear Physics, Contract No. DE-AC02-06CH11357.

- 
- [1] G. Montagnoli, A. M. Stefanini, H. Esbensen, C. L. Jiang, L. Corradi, S. Courtin, E. Fioretto, J. Grebosz, F. Haas, H. M. Jia, M. Mazzocco, C. Michelagnoli, T. Mijatović, D. Montanari, C. Parascandolo, F. Scarlassara, E. Strano, S. Szilner, and D. Torresi, *Phys. Rev. C* **90**, 044608 (2014).
  - [2] C.L. Jiang, B. B. Back, H. Esbensen, J. P. Greene, R. V. F. Janssens, D. J. Henderson, H. Y. Lee, C. J. Lister, M. Notani, R. C. Pardo, N. Patel, K. E. Rehm, D. Seweryniak, B. Shumard, X. Wang, S. Zhu, Ş.Mişicu, P. Collon, and X. D. Tang, *Phys. Rev. C* **78**, 017601 (2008).
  - [3] C. L. Jiang, H. Esbensen, K. E. Rehm, B. B. Back, R.V. F. Janssens, J. A. Caggiano, P. Collon, J. Greene, A. M. Heinz, D. J. Henderson, I. Nishinaka, T. O. Pennington, and D. Seweryniak, *Phys. Rev. Lett.* **89**, 052701(2002).
  - [4] N. J. Stone, *At. Data Nucl. Data Tables*, **90**, 75 (200).
  - [5] E. Bozek, D.M. De Castro-Rizzo, S. Cavallaro, B. Delaunay, J. Delaunay, H. Dumont, A. D’Onofrio, M.G. Saint-Laurent, L. Sperduto, F. Terrasi, *Nucl. Phys. A* **451**, 171 (1986).
  - [6] G. Colucci, G. Montagnoli, M. Faggian, A. Goasduff, M. Mazzocco, F. Scarlassara, C. Stefanini, E. Strano, M. Urbani, A. M. Stefanini, L. Corradi, E. Fioretto, F. Galtarossa, G. L. Zhang, D. Bourgin, S. Courtin, F. Haas, P. Colović, S. Szilner, *Proc. Int. Nucl. Phys. Conf., Adelaide (Australia)*, 11-16 Sept. 2016, *PoS INPC2016*, 220 (2017).
  - [7] G. Colucci, G. Montagnoli, A.M. Stefanini, D. Bourgin, P. Čolović, L. Corradi, S. Courtin, M. Faggian, E. Fioretto, F. Galtarossa, A. Goasduff, F. Haas, M. Mazzocco, F. Scarlassara, C. Stefanini, E. Strano, M. Urbani, S. Szilner, and G.L. Zhang *Proc. Int. Conf. on Heavy-Ion Collisions at Near-Barrier Energies*, Hobart, (Tasmania, Australia) Feb. 20-24, 2017, *Eur. Phys. J. Web of Conf.* **163**, 00010 (2017).
  - [8] G. Montagnoli, A. M. Stefanini, C. L. Jiang, H. Esbensen, L. Corradi, S. Courtin, E. Fioretto, A. Goasduff, F. Haas, A. F. Kifle, C. Michelagnoli, D. Montanari, T. Mijatović, K. E. Rehm, R. Silvestri, Pushpendra P. Singh, F. Scarlassara, S. Szilner, X. D. Tang, and C. A. Ur, *Phys. Rev. C* **85**, 024607 (2012).
  - [9] J. X. Wei, J. R. Leigh, D. J. Hinde, J. O. Newton, R. C. Lemmon, S. Elfstrom, J. X. Chen and N. Rowley, *Phys. Rev Lett.* **67**, 3368 (1991).
  - [10] A. M. Stefanini, D. Ackermann, L. Corradi, D. R. Napoli, C. Petrache, P. Spolaore, P. Bednarczyk, H. Q. Zhang, S. Beghini, G. Montagnoli, L. Mueller, F. Scarlassara, G. F. Segato, F. Soramel and N. Rowley *Phys. Rev Lett.* **74**, 864 (1995).
  - [11] Ö.Akyüz and Å.Winther, in *Nuclear Structure and Heavy-Ion Physics*, *Proc. Int. School of Physics “Enrico Fermi”*, Course LXXVII, Varenna, edited by R.A.Broglia and R.A.Ricci (North Holland, Amsterdam, 1981)
  - [12] Ş. Mişicu and H. Esbensen, *Phys. Rev. C* **75**, 034616 (2007).
  - [13] G. Montagnoli, A.M. Stefanini, H. Esbensen, L. Corradi, S. Courtin, E. Fioretto, J. Grebosz, F. Haas, H.M. Jia, C.L. Jiang, M. Mazzocco, C. Michelagnoli, T. Mijatović, D. Montanari, C. Parascandolo, F. Scarlassara, E. Strano, S. Szilner, D. Torresi, *Phys. Lett. B* **746**, 300 (2015).
  - [14] I. Angeli, *At. Data and Nucl. Data. Tables*, **87**,185 (2004).
  - [15] H. Esbensen, *Phys. Rev. C* **85**, 064611 (2013).
  - [16] S. Gary and C. Volant, *Phys. Rev. C* **25**, 1877 (1982).